JACS
JOURNAL OF THE AMERICAN CHEMICAL SOCIETY
Article
pubs.acs.org/JACS

Structural Diversity and Electron Confinement in Li_4N: Potential for 0-D, 2-D, and 3-D Electrides

Yuta Tsuji,[†] Prasad L. V. K. Dasari,[*,‡] S. F. Elatresh,[§] Roald Hoffmann,[*,§] and N. W. Ashcroft[∥]

[†]Education Center for Global Leaders in Molecular Systems for Devices, Kyushu University, Nishi-ku, Fukuoka 819-0395, Japan
[‡]Department of Chemistry, Indian Institute of Technology, Kanpur 208016, India
[§]Department of Chemistry and Chemical Biology, Baker Laboratory, Cornell University, Ithaca, New York 14853, United States
[∥]Laboratory of Atomic and Solid State Physics, Cornell University, Ithaca, New York 14853, United States

Supporting Information

ABSTRACT: In pursuit of new lithium-rich phases and potential electrides within the Li−N phase diagram, we explore theoretically the ground-state structures and electronic properties of Li_4N at P = 1 atm. Crystal structure exploration methods based on particle swarm optimization and evolutionary algorithms led to 25 distinct structures, including 23 dynamically stable structures, all quite close to each other in energy, but not in detailed structure. Several additional phases were obtained by following the imaginary phonon modes found in low-energy structures, as well as structures constructed to simulate segregation into Li and Li_3N. The candidate Li_4N structures all contain NLi_n polyhedra, with n = 6−9. They may be classified into three types, depending on their structural dimensionality: NLi_n extended polyhedral slabs joined by an elemental Li layer (type **a**), similar structures, but without the Li layer (type **b**), and three-dimensionally interconnected NLi_n polyhedra without any layering (type **c**). We investigate the electride nature of these structures using the electron localization function and partial charge density around the Fermi level. All of the structures can be characterized as electrides, but they differ in electronic dimensionality. Type-**a** and type-**b** structures may be classified as two-dimensional (2-D) electrides, while type-**c** structures emerge quite varied, as 0-D, 2-D, or 3-D. The calculated structural variety (as well as detailed models for amorphous and liquid Li_4N) points to potential amorphous character and likely ionic conductivity in the material.

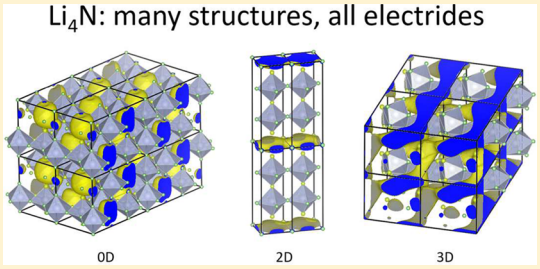

INTRODUCTION

We suggest in this paper that a metastable solid of composition Li_4N is likely to exist, possibly amorphous at standard temperature and pressure, and that this material may in several modifications provide us with examples of a P = 1 atm electride of varying dimensionality.

To begin, let us examine what is known about the lithium−nitrogen phase diagram, electrides, and why one might expect Li_4N to be an electride.

Li−N Compounds, Experimental. Under standard conditions, two crystalline lithium−nitrogen compounds are well known, namely Li_3N (nitride)[1] and LiN_3 (azide).[2] Li_3N, the expected ionic composition, dominates the Li−N phase diagram.[3,4] There is some disagreement between theory and experiment on its structure, to which we will return. In contrast to the nitride, we have LiN_3, containing the common NNN azide anion, a metastable, reactive, energy-rich, and indeed explosive compound.[5,6]

Recently, another lithium−nitrogen compound, Li_2N_2 (diazenide),[7] was synthesized by controlled thermal decomposition of ionic azides in a multi-anvil device under high-pressure/high-temperature conditions, followed by returning the material to 1 atm and room temperature. Li_2N_2 is intermediate between Li_3N and LiN_3: featuring well-separated molecular diazenide units $(N_2)^{2-}$, it joins a small group of reduced dinitrogen compounds.[8]

LiN_3 contains Li^+ and molecular linear azide ions (N_3^-), while Li_3N predictably features N^{3-}, leading to one of the most ionic nitrides known. As expected, both compositions are insulators. However, Li_3N shows high ionic conductivity, of the order of 10^{-3} Ω^{-1} cm^{-1} at room temperature,[9] due to rapid diffusion of Li^+ ions caused by strong anharmonic thermal vibrations.[10] Conductivity measurements showed that Li_2N_2 is, unusually, both an electronic and an ionic conductor.[11]

To understand lithium corrosion phenomena, the solubility of non-metals in liquid lithium has been widely investigated.[12] At temperatures above 400 °C, the solubility decreases in the order N > H > C > O > F.[13] Nitrogen thus shows very high solubility in lithium. The Li−N phase diagram has been much investigated experimentally,[13,14] and well used in thermodynamic modeling.[15]

Theory and Li−N Phases. There exist various algorithms for generating optimum crystal structures.[16] Last year, two groups independently published a convex-hull diagram (an especially convenient way of summarizing thermodynamic

Received: August 30, 2016
Published: September 26, 2016

DOI: 10.1021/jacs.6b09067
J. Am. Chem. Soc. 2016, 138, 14108−14120

preferences) for the lithium−nitrogen system under both standard and high pressures.[17,18] Ma and co-workers[17] used a structure search method based on the swarm-optimization CALYPSO algorithm.[19] Oganov and co-workers[18] used their variable-composition evolutionary structure prediction tool, the USPEX algorithm.[20] Zunger and co-workers had already performed a structure search for the sodium−nitrogen system by using a global space-group optimization approach,[21] and the convex-hull diagram obtained is quite similar to that of the lithium−nitrogen system.

The existing theoretical searches recover the known nitride as the most stable compound over a range of pressures. The convex-hull diagram also shows that LiN_3 should be thermodynamically unstable at standard pressure.[17,18] Metastable as the azide is, it can be made. On the N-rich side of the Li−N phase diagram, the structure searches have predicted that $P6_3/mmc$ LiN_2 should also be a thermodynamically stable compound.[17,18]

Electrides. Electrides are generally defined as ionic compounds in which anionic electrons reside in the interstitial locations or voids of a host lattice.[22] This form of matter is relatively uncommon, but well characterized. Several electrides are known at 1 atm,[23−29] and more are predicted or observed in high-pressure experiments, mainly in high-pressure allotropes of elements (Li,[30] C,[31] Na,[32] Cs,[33] Mg,[34] etc.). A common occurrence in ionic crystals is that of F-centers or color centers—anionic vacancies filled by one or two electrons.[35] A chemical and physical theory of high-pressure electrides has been proposed recently.[36,37]

Though it is common to think of electrides as solids, we could extend the definition to liquids, as well. The history of electrides then can be traced further back, to Davy's observation of the blue or bronze color of alkali metal−ammonia solutions in 1808.[29,38,39] No one who has seen these colors can forget them. The color is due to solvated electrons and $Li(NH_3)_4$ molecules.[40] We, therefore, see Davy's alkali metal−ammonia solutions within the electride universe.

In 1983, Dye and co-workers[41] succeeded in the synthesis of a crystalline organic electride, where the isolation of electrons is achieved by the complexation of alkali cations by crown ethers or cryptands.[24] At room temperature, these compounds degrade rapidly.[42] But this problem was overcome, and a thermally stable organic electride was synthesized by employing a per-aza analogue of the cryptand.[43]

In 2002, Dye and co-workers also succeeded in the synthesis of a thermally stable inorganic electride by inserting cesium into zeolite ITQ-4.[44] This electride is predicted to be metallic.[45] The year after, Hosono and co-workers synthesized another inorganic electride based on a ceramic material (a mayenite-type oxide), namely $12CaO{\cdot}7Al_2O_3$ (referred to as C12A7).[46] They extracted the encapsulated O^{2-} ions by using a metal such as Ca via oxide formation from the sub-nanometer-sized cages formed by Ca, Al, and O ions, resulting in a thermally stable electride. C12A7 shows metallic conductivity (100 S cm^{-1} at 300 K)[46] arising from cage-to-cage electron hopping (tunneling).[47]

The composition Li_4N which we will explore in this paper is a formally "isoelectronic" analogue to Ca_2N, which is an interesting alkaline earth (AE) metal−nitrogen system, a so-called sub-nitride, and a well-studied electride.[27,48] Ca_2N has a layered structure, made up of edge-sharing NCa_6 octahedra (anti-$CdCl_2$ structure-type) with a N−Ca distance of 2.44 Å.[27] Two-dimensionally confined anionic electrons are found in the interlayer region. Other AE metal sub-nitrides, such as Sr_2N and Ba_2N, have the same crystal structure and are also predicted to be electrides.[49] As far as we can tell, alkali metal (A) sub-nitrides (A_4N or higher) are not known under ambient conditions. However, $Li_{15}N$ and Li_5N compositions are predicted to be stable under high pressure.[18] There is also a theoretical study of the metastability of gas-phase perlithiated molecules, such as Li_4N and Li_5N.[50] As will emerge in our study, Li_4N adopts a form analogous to the known Ca_2N-type structure, but with interesting structural differences.

One can classify electrides into zero-dimensional (0-D), 1-D, and 2-D on the basis of the dimensionality of the electronic structure of the anionic electrons as well as the geometric structure of the space where they are trapped. The 0-D electride is exemplified by C12A7 (see above), in which the anionic electrons are localized at interstitial sites and should therefore lead to a narrow band, the so-called *cage states* or *cage conduction band*.[51] The 2-D electride is exemplified by Ca_2N, in which the anionic electrons are loosely confined in the interlayer space and behave as a 2-D electron gas, resulting in a broad band. Recently, a combined experimental and theoretical study conducted by Hosono and co-workers has added Y_2C to the family of 2-D electrides.[52] 1-D electrides are not known, but Hosono and co-workers predict a 1-D electride with a $[La_8Sr_2(SiO_4)_6]^{4+}{:}4e^-$ configuration, in which the four anionic electrons are confined in the channel spaces of the host material.[53] Recently they also investigated a quasi-1-D electride with the formula Y_5Si_3.[54]

The low-dimensionally confined electrons in the interstitial voids of electrides lead to many fascinating chemical and physical properties, such as a low work function, i.e., 2.4−2.6 eV, which is less than those of alkali and alkaline-earth metals.[55,56] Building on such properties, C12A7 and Ca_2N electrides have been used as electron injectors in various applications, such as catalysts[57−61] and electronic devices.[62] Also, application to non-linear optical materials,[63,64] anode materials,[65] and superconductors[66,67] is envisaged.

Theorists have been active in exploring electrides. Liu and co-workers, using the CALYPSO structure-searching methodology, found that Li−C compounds are likely to be 2-D electrides.[68] Hosono and co-workers[69,70] have carried out extensive database screening followed by density functional theory (DFT) calculations and identified some carbides as likely 2-D electrides. Ma and co-workers have designed 89 new inorganic electrides that are classified into 3-D, 2-D, and 0-D by what they call inverse design.[71]

Most of the searching for electrides has been carried out for high pressure, and under those conditions Mg_3O_2,[72] Na_2He,[73] and Li_6O[74] have been identified as electrides. Recently, Kokail et al. have found an electride-like interstitial charge localization in Li−S compounds under high pressure.[75] Also, there are some theoretical studies on single molecules as possible electrides.[76−78] One needs great theoretical care here, as one does in the more developed field of Rydberg molecules.[79] Development of theoretical methodology to quantify electron delocalization and describe electronic structure in electrides also plays an important role.[80,81]

As we will show, Li_4N, or $[(Li^+)_4N^{3-}{\cdot}e^-]$, electrides are predicted to contain voids of varying dimensionality, very much akin to the C12A7 and Ca_2N materials. In the Li−Li_3N phase diagram, a smooth liquidus extends across the entire composition range, and there is no experimental evidence for a eutectic.[13] The investigation that follows provides evidence

DOI: 10.1021/jacs.6b09067
J. Am. Chem. Soc. 2016, 138, 14108−14120

for metastable solid Li_4N, perhaps crystalline, perhaps amorphous (a glassy state).

RESULTS AND DISCUSSION

Li_3N Crystal Structures. Given the great stability of ionic Li_3N in the Li−N phase diagram, we might anticipate in Li_4N an intergrowth of layers or slabs, or 3-D ionic regions, resembling the nitride structure, along with metallic Li regions, as can be seen in the alkali metal sub-oxides.[82] Therefore, before we scrutinize Li_4N, let us review the structure of Li_3N.

Experimentally Li_3N, α-Li_3N, has been characterized as a hexagonal layered *P6/mmm* structure (see Figure 1a) at

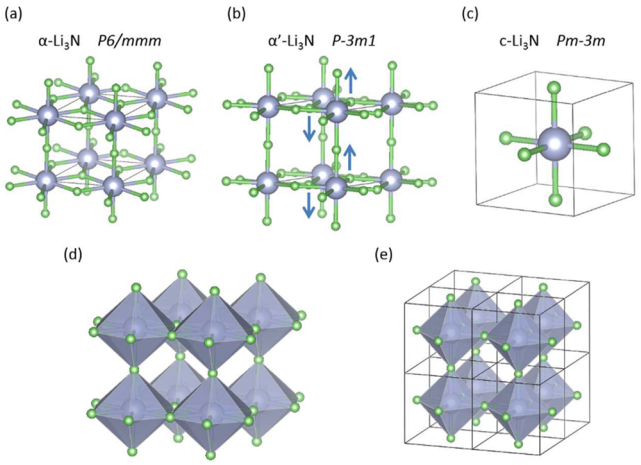

Figure 1. Optimized structures of (a) α-Li_3N, (b) α'-Li_3N, and (c) c-Li_3N [green = Li, purple = N]. Since the geometrical difference between α-Li_3N and α'-Li_3N is very small, blue arrows indicating slight distortions of Li atoms along the *c*-axis are shown as a guide to the eye. Polyhedral representations for α-Li_3N and c-Li_3N are also shown in (d) and (e), respectively.

standard pressure.[10] However, recent theoretical studies found that the α-Li_3N structure has an imaginary phonon mode under static conditions and as $T \rightarrow 0$ K; further searching then leads to a $P\bar{3}m1$ α'-Li_3N structure (see Figure 1b).[83] Not only is the energy difference of the two structures tiny (around 1 meV/formula unit), but also the geometrical difference between them is small.[83] One of the aforementioned structure searches, that of Oganov and co-workers,[18] found a competitive cubic structure of Li_3N (c-Li_3N), with space group $Pm\bar{3}m$, at 0 GPa (see Figure 1c). Jansen and co-workers[84] predicted the c-Li_3N structure should be a metastable phase with a very small transition pressure relative to the α-Li_3N structure. c-Li_3N has no imaginary phonon modes, is semiconducting with a calculated band gap of 1.90 eV, and has in these calculations a lower formation enthalpy than α-Li_3N and α'-Li_3N by around 25 meV/formula unit.[85] In the Supporting Information (SI) we discuss our own calculations on the three Li_3N structures. Functionals make a difference, but all three structures are very close to each other in energy.

Although there are slight displacements of Li atoms along the *c*-axis (around 0.1 Å), indicated by blue arrows in Figure 1b, α-Li_3N and α'-Li_3N are quite similar in structure. The N^{3-} ions have two Li neighbors at 1.9 Å and six at 2.1 Å, forming corner- and edge-sharing NLi_8 polyhedra (hexagonal bipyramids, see Figure 1d). The variation in N−Li distances is very small, and actually not far from the sum of the Shannon radii[86] for the ions (1.46 Å for N^{3-}, 0.76 Å for Li^+). Li atoms in the basal plane are shared by three N atoms, while the other Li atoms in apical positions are shared by two N atoms. On the other hand, in c-Li_3N, the nitride ions have six Li neighbors at 1.9 Å, forming corner-sharing NLi_6 octahedra (see Figure 1e), where all Li atoms are shared by two N atoms. This structure is akin to that of Na_3N,[84,87] which has the so-called anti-ReO_3 structure.

The polyhedral representation makes clear the difference between c and α, α' structures for Li_3N: the first coordination sphere of the nitride contains six lithiums in one case and eight in the other. They are quite different, yet both close to each other in energy. The similarity in energy of two or three structures differing from each other not in the position of the nitrides, but in the position of the Li^+ ions, of course must be related to the eventual ionic conductivity of solid Li_3N. N-centered NLi_n polyhedral units will also emerge as the key structural motif in Li_4N.

Li_4N Crystal Structures. To find stable structures of Li_4N at P = 1 atm, we performed static ground-state structure searches using both an evolutionary algorithm, as implemented in the XtalOpt program,[88] and particle-swarm optimization, which is implemented in the CALYPSO program.[19] All the calculations reported in this paper are ground-state calculations at P = 1 atm. The phonons and zero-point energies (ZPEs) are primarily calculated using the harmonic approximation. We are working on moving beyond this approximation.

Too many structures, close in energy yet distinct, came our way. Some of them are very similar. We screened these structures on the basis of the type of the NLi_n polyhedra they contain, their connectivity, histograms of atom-to-atom distances, space group, lattice parameter, and total energy. We found in the end some 25 distinct structures, including 22 dynamically stable structures, which are summarized in Table 1, and three dynamically unstable structures, within 18 meV/atom of each other in energy. Note that structure **1** in Table 1 was not found in our initial structure search, but we came to it in another way, to be described. Some of the structures in the table were found by both XtalOpt and CALYPSO, but the others were only found by either XtalOpt or CALYPSO.

In Table 1, the enthalpy of formation (ΔH_f) of Li_xN_y is calculated using the following formula:

$$\Delta H_f(Li_xN_y) = [H(Li_xN_y) - xH(Li) - yH(N)]/(x + y) \quad (1)$$

where the enthalpies of α-N ($Pa\bar{3}$)[89] and bcc Li ($Im\bar{3}m$)[90] are used as a reference. Although Li has a bcc structure under ambient conditions, it undergoes a martensitic phase transition at around 75 K from bcc to a rhombohedral 9R ($R\bar{3}m$) structure, which is a close-packed structure with a nine-layer stacking sequence.[91,92] Our calculation using the PBE functional showed that the 9R Li is little bit more stable than the bcc Li, by 1.5 meV/atom. This value is not far from the values found in the literature.[93,94] Even if dispersion correction and HSE06 hybrid functional calculation are included, the energy difference between bcc and 9R remains almost unaffected (the SI contains a detailed discussion of corrections for ZPE, the inclusion of dispersion, and the effects of a hybrid functional). However, the ZPE of 9R is larger than that of bcc by just 1.4 meV/atom in the harmonic approximation, so they have almost the same energy after the ZPE correction. Were we to adopt the 9R Li as the reference for the calculation of the formation enthalpy of Li_4N structures without any ZPE correction, the enthalpies of the latter would be larger by 1.2 meV/atom.[95] It

DOI: 10.1021/jacs.6b09067
J. Am. Chem. Soc. 2016, 138, 14108−14120

Table 1. Dynamically Stable Li_4N Structures Obtained[a]

structure	Z	space group	ΔH_f (eV/atom)[b]	type[c]	type of polyhedra[d]	connectivity of polyhedra
1	8	*Pmma*	−0.309	**a**	NLi_6	corner
2	2	*P4/mmm*	−0.305	**a**	NLi_6	corner
3	4	$P2_1/c$	−0.301	**b**	NLi_8	corner, edge
4	8	*Fmmm*	−0.299	**c**	NLi_8	corner, edge
5	8	*C2/c*	−0.298	**b**	NLi_8	corner, edge
6	4	*Cmcm*	−0.295	**b**	NLi_7	corner, edge
7	4	*P1*	−0.293	**b**	NLi_7, NLi_8	corner, edge
8	3	*P1*	−0.292	**c**	NLi_8	corner, edge, face
9	4	*C2/m*	−0.292	**c**	NLi_7	corner, edge
10	6	$R\bar{3}m$	−0.292	**a**	NLi_8	corner, edge
11	2	$P\bar{6}m2$	−0.291	**a**	NLi_8	corner, edge
12	4	*P1*	−0.290	**b**	NLi_7, NLi_8	corner, edge
13	3	*P3m1*	−0.290	**a**	NLi_8	corner, edge
14	4	*Pc*	−0.289	**b**	NLi_6, NLi_8	corner, edge
15	4	$P\bar{1}$	−0.289	**b**	NLi_9	edge, face
16	4	$P\bar{1}$	−0.289	**b**	NLi_8	corner, edge, face
17	8	*C2/m*	−0.289	**c**	NLi_8, NLi_9	corner, edge, face
18	8	*Cmcm*	−0.289	**c**	NLi_7	corner, edge
19	8	*Cc*	−0.289	**c**	NLi_8, NLi_9	edge, face
20	2	*C2/m*	−0.288	**b**	NLi_8	edge
21	2	$P6_3mc$	−0.288	**b**	NLi_8	edge
22	4	$P2_1/c$	−0.287	**b**	NLi_9	edge
23	3	*P1*	−0.287	**c**	NLi_8	corner, edge, face

[a]Except for structure **1**, they were found in our structure search. Structure **1** was arrived at by following the imaginary phonon modes in a dynamically unstable structure of low energy. See text for details. [b]Calculated by using the PBE functional without zero-point energy (ZPE) correction. [c]The structural classification is given in the text. Briefly, type-**a** structures contain NLi_n extended polyhedral slabs joined by Li parallelogram sub-lattices, type-**b** structures contain NLi_n extended polyhedral slabs joined by void slabs, and type-**c** structures contain what appear to be 0-D voids. [d]On examining all the histograms of N−Li distances, we found that the longest N−Li distance in the quite distinct first coordination peak is at 2.4 Å. So we set this distance to be the threshold for determining the coordination polyhedron around a nitride ion.

is, of course, important what the ground-state structure of Li actually is, but for our energetic considerations on Li_4N, whether the reference energy of Li is for bcc or 9R is not significant.

Figure 2a shows the energetically most stable structure found in our structure search (denoted as **1′**). But let us immediately add that it is so by only 4 meV per atom (20 meV per formula unit) compared to the second most stable one. Structure **1′** is not included in Table 1 because it is found to be dynamically unstable (see below for details). In this *P4/mmm* structure, $Z = 4$, where Z is the number of formula units per unit cell. We can see in the structure of **1′** a four-layered corner-sharing NLi_6 octahedral slab as well as Li square sub-lattices. There are three Li atoms in the interlayer region, which appear to have no interaction with N atoms. They might be regarded as an elemental Li layer, whose structure is similar to bcc Li. The four-layered corner-sharing NLi_6 octahedral slab in this structure is identical to a slab of the cubic structure of Li_3N (c-Li_3N). This suggests that we should worry about possible larger unit cell segregations, on the way to bcc Li + c-Li_3N.

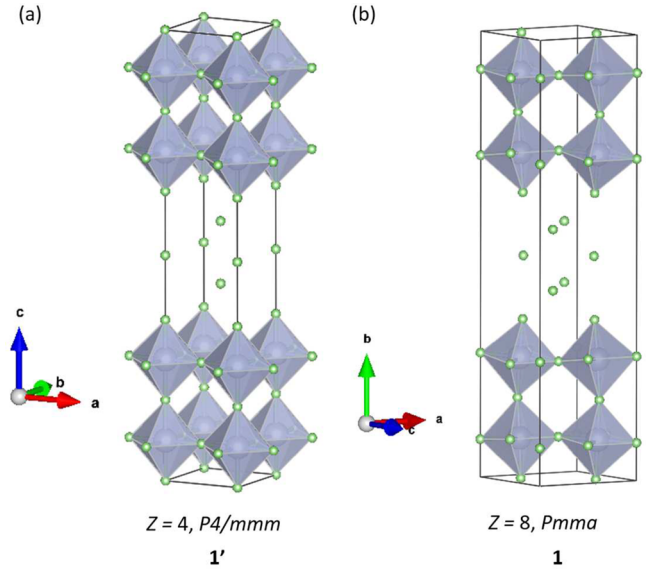

Figure 2. (a) Calculated $Z = 4$, *P4/mmm* structure of Li_4N with the lowest energy in our initial structure search (structure **1′**). This structure has small imaginary phonon modes. (b) $Z = 8$, *Pmma* structure of Li_4N (structure **1**), which was obtained by following the imaginary phonon modes in the $Z = 4$, *P4/mmm* structure. The N-centered NLi_6 octahedral units are illustrated in polyhedral representation. In this and all subsequent figures we show static ground-state structures.

Though we do not have the computational resources to do structure searches for the structures with larger Z values than 4, we did explore potential segregation in another way (see below).

Our phonon calculation revealed that the $Z = 4$, *P4/mmm* structure has imaginary phonon modes, indicating dynamical instability. So we followed the imaginary phonon modes and reached a little bit more stable structure (structure **1**), with no imaginary phonons. The energy difference between the two structures is just 1 meV/atom. The *Pmma* structure obtained is shown in Figure 2b; it has $Z = 8$. Clearly this is a slightly distorted version of $Z = 4$, *P4/mmm* structure.

Let us look at other stable structures. Figure 3 shows the second, third, and fourth most stable structures found in our structure search (structures **2**, **3**, and **4**). In this figure, energies relative to structure **1** are also shown. These structures are energetically very close to the most stable one just described, yet they are geometrically *very* different from that structure and each other. Perhaps this is most easily seen from a structural fingerprint, a histogram of N−Li and Li−Li distances in the two structures, in Figure 3. Note that the histograms are for all N or Li atoms in unit cell, so if one wants the number of them per N or Li atom, one has to divide by Z, and further by 4 for Li. Histograms of N−N separations (not shown) are not informative—in all structures the nitride ions keep as far away from each other as possible, at a N−N separation of 3.5−4.0 Å.

The peaks in the histograms of N−Li separations are very discrete. The first peak, which describes the first coordination sphere of N, is observed around 2.0 Å. This value is pretty much the same as the N−Li distances in Li_3N, and is very close to the sum of the Shannon radii for N^{3-} and Li^+. The major variation in the Li−N histograms is in the number of atoms in the first coordination sphere, namely the number of lithiums

DOI: 10.1021/jacs.6b09067
J. Am. Chem. Soc. 2016, 138, 14108−14120

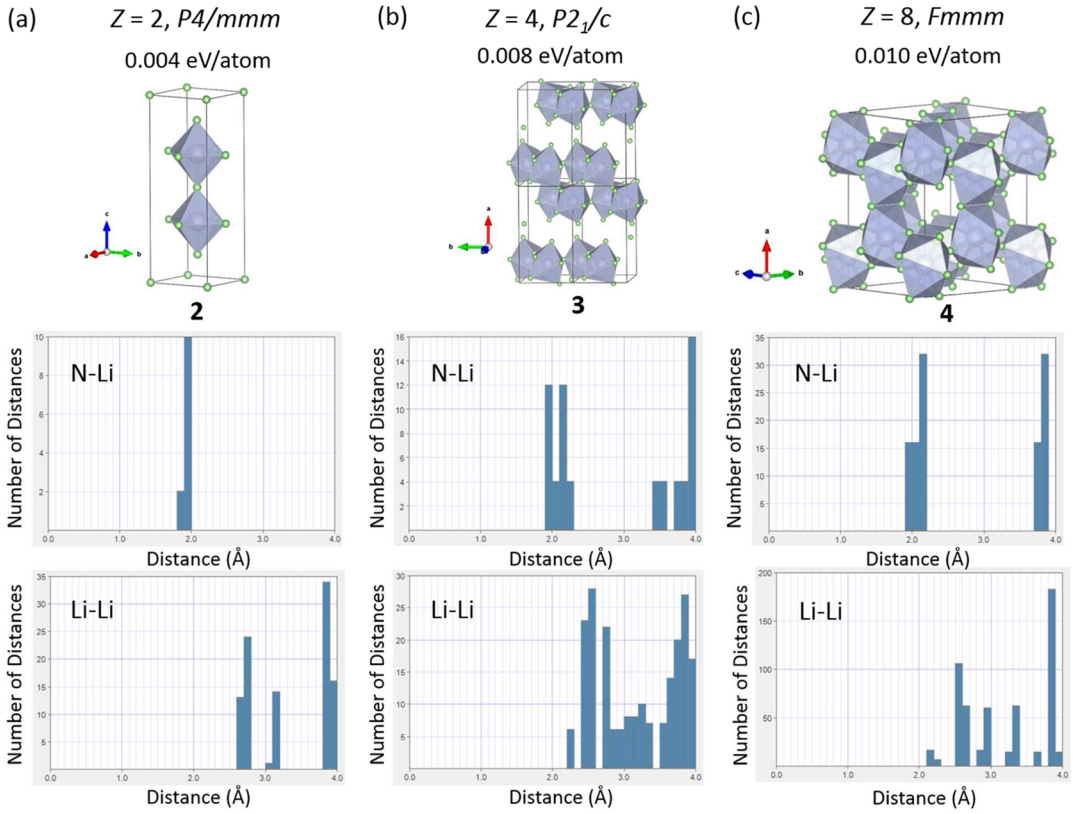

Figure 3. (Top) The second (a), third (b), and fourth (c) most stable structures of Li_4N found in our structure search (structures **2**, **3**, and **4**, respectively). *Z*, space group, and the energy relative to structure **1** are shown above each structure. (Middle) Histograms of the distances from all N atoms in the unit cell to Li atoms and (bottom) those from all Li atoms in the unit cell to the other Li atoms. The histograms were generated by Distance Explorer implemented in CrystalMaker. The distance search was carried out in the range from 0 to 4 Å. The bin size is set to 0.1 Å.

about the same short distance from the nitride. This is 6 for the lowest energy structure, and 6 for the first structure in Figure 3a, but it is 8 for the other two structures in Figure 3. The histogram of Li−Li separations strongly depends on the structure, so this is a really good structural fingerprint.

The *Z* = 2, *P*4/*mmm* structure (structure **2**, Figure 3a) goes out of dynamical stability if we use much finer k-point grids and/or a much larger supercell in the phonon calculations. Following the imaginary phonon modes leads to a *Z* = 4, *Pmma* structure (shown in the SI). There is no discernible energy difference between the two structures; the accompanying distortions are small. We will retain the higher symmetry structure in the discussion. Let us call this class of crystal structures, of which **1**′ and **2** are examples, type **a**, namely those structures containing NLi_n extended polyhedral slabs joined by Li parallelogram sub-lattices.

In the $P2_1/c$ structure (structure **3**, Figure 3b), we can clearly see layering. The layer consists of corner- and edge-sharing NLi_8 polyhedra. There are no isolated Li atoms in the interlayer region; instead one can perceive void slabs. All the lithiums are within the first coordination sphere of a nitrogen. Let us call this class of crystal structures type **b**, the class containing NLi_n extended polyhedral slabs joined by what we may call void slabs. This structure type is analogous to the known Ca_2N-type.

Our structure search was performed in the range of *Z* from 1 to 4, but we can generate a conventional cell, which has a *Z* larger than 4, based on the symmetry of the primitive cell obtained. Thus, Figure 3c shows an *Fmmm* structure that has *Z* = 8 (structure **4**). This structure is composed of corner- and edge-sharing NLi_8 polyhedra. Since the polyhedral units are three-dimensionally interconnected, we do not see any layering. Let us call this class of crystal structures type **c**.

The voids included in type-**b** structures are two-dimensionally extended. On the other hand, the dimensionality of the voids, judged structurally, in type-**c** structures has to be determined individually. For example, in the middle of the unit cell of structure **4**, a void can be perceived; it has fairly big passages to neighboring voids along four directions in the *bc* plane, pointing from the center of the cell to the midpoint of the "**a** edge". This suggests that the voids in **4** are extended two-dimensionally. It is hard to decide whether the passage between two neighboring voids is large or small, so one might argue that the voids in **4** are 0-D. Later we will judge the dimensionality of these type-**c** structures in another, electronic, way based on the electron distribution near the Fermi level.

The last two structures in Figure 3, though they contain NLi_8 polyhedra, are different from those found in α-Li_3N and α'-Li_3N (these contain hexagonal bipyramids). Among our 23 dynamically stable Li_4N structures, we found some that are akin to α-Li_3N and α'-Li_3N. These are structures **10** and **20**, shown in the SI.

All the other structures we found, while different from each other and distinct—and this distinction is most easily seen in their fingerprint histograms, shown in the SI—can be classified into the three types identified. All the indications are of a good number of competitive structures of comparable energy. The resulting material may well be amorphous, a possibility we investigate in more detail below.

Is Li_4N Stable? Figure 4 illustrates the enthalpy of formation per atom for the reaction $xLi + yN \rightarrow Li_xN_y$

DOI: 10.1021/jacs.6b09067
J. Am. Chem. Soc. 2016, 138, 14108−14120

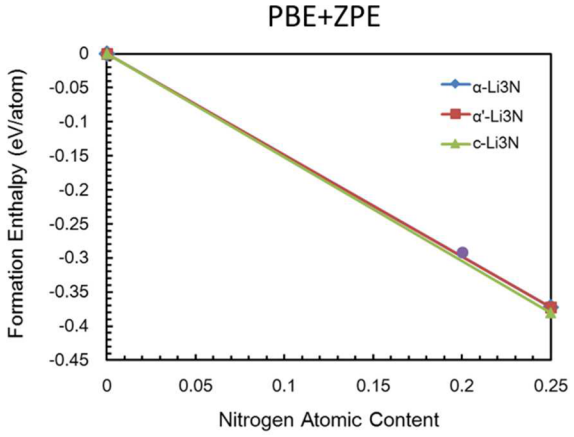

Figure 4. Part of the convex-hull diagram of the Li−N binary system, namely the tie-lines between bcc Li and α-, α'-, and c-Li_3N, as a function of nitrogen atomic content. Enthalpies of formation (ΔH_f) per atom of static ground-state Li_xN_y phases at P = 1 atm and $T \rightarrow 0$ K are calculated with the PBE functional; harmonic ZPEs are added. The purple filled circle indicates ΔH_f of the most stable Li_4N found, structure **1**.

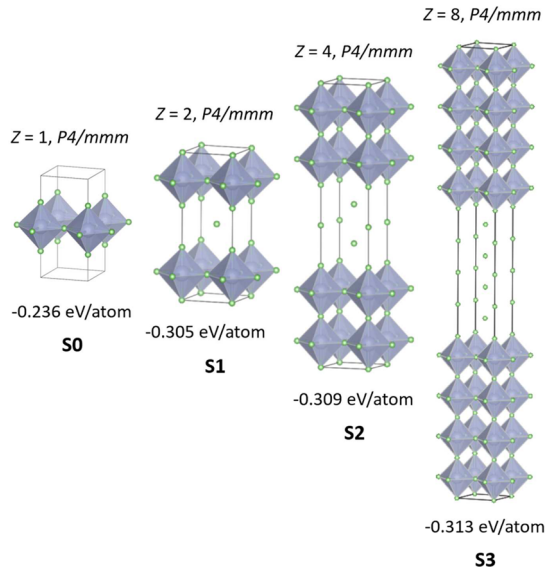

Figure 5. Sequence probing segregations of Li_4N into the c-Li_3N and bcc Li layers. **S1** is the same as the structure **2**, but with a different choice of cell origin. **S2** is the same as the structure **1′** shown in Figure 2a. **S3** is the structure constructed from **S2** (see the text for the details of the construction). We start the process with a less segregated structure with Z = 1, **S0**. The formation enthalpy calculated with the PBE functional without ZPE is shown below the structure.

calculated with eq 1, as a function of nitrogen atomic content, i.e., $y/(x + y)$, in the range from 0 to 0.25. Note that ZPE energies *are* included. The SI shows similar lines for inclusion of dispersion corrections, and for single-point HSE06 computations.

The leftmost point on the horizontal axis corresponds to bcc Li. We need to connect the tie line to the energy of Li_3N, and here we run into the problem encountered earlier—there is disagreement, between experiment and theory, and also among the theoretical treatments, on whether the favored structure is α-Li_3N, α'-Li_3N, or even c-Li_3N. We draw lines to all three in Figure 4; it can be seen that the Li_3N energies are so close to each other that the question of which structure one is to use is effectively moot.

In Figure 4, the purple filled circle indicates ΔH_f of the most stable Li_4N structure. The circle essentially touches the line. Li_4N is thermodynamically stable, or very close to it—its decomposition to Li and the nitride is approximately thermoneutral at P = 1 atm.

Possibility of Segregation into c-Li_3N and bcc Li. Structures **1**, **2**, and **10** hint at a segregation to Li + c-Li_3N or Li + $\alpha(\alpha')$-Li_3N. This has to be investigated further. As we mentioned above, for Z = 2, $P4/mmm$ (**2**) and Z = 4, $P4/mmm$ (**1′**) structures can be perceived as built up of alternating c-Li_3N and bcc Li layers. Here we will call them structures **S1** and **S2**.

We cannot do full structure searches for $Z > 4$. To check whether further segregation leads to still more stabilization, we adopted a different strategy. We constructed manually a doubled unit cell of **S2** in the direction of the c-axis. Then, the central c-Li_3N layer was divided into two, and the upper half was exchanged with the bcc Li layers located just above it. The same thing was done for the lower half. This trial structure was optimized; the result is shown in Figure 5. We call this structure **S3**.

We can also manually generate a less segregated structure with Z = 1 as a starting model of probing segregation. This structure does not contain any Li atoms between the NLi_6 polyhedral slabs. We call this structure **S0**. From a phonon calculation, this structure is found to be dynamically unstable (see the SI).

The formation enthalpy without ZPE of **S3** is −0.313 eV/atom. This is more stable, by just a little, than any other structure found in our structure search. Since this enthalpy does not include ZPE, we cannot update the position of the purple filled circle in Figure 4. But it should definitely be on the tie-line calculated without ZPE correction shown in the SI.

At the first step of the segregation (from **S0** to **S1**), the structure is significantly stabilized by 69 meV/atom. However, after that, at each step of the segregation sequence (from **S1** to **S2** or from **S2** to **S3**), the structure becomes more stable just by 4 meV/atom. We do not have the computational resources at present for calculating phonons of **S3**; if it is dynamically unstable, there is a still more stable (slightly, judging by our experience with other structures) structure to be found.

There is a good reason why segregation is a possibility. First, both Li and Li_3N have a cubic unit cell. Second, the lattice parameters of bcc Li and c-Li_3N are very close. $a = b$ = 3.42 Å for bcc Li, and $a = b$ = 3.87 Å for c-Li_3N. The segregated structures have an intermediate lattice parameter of $a = b$ = 3.85 Å, and thus the resulting structures emerge as a compromise between them, since the lattice spacing in the composite is closer to that of c-Li_3N, bcc Li seems to be softer than the ionic nitride. Of course this line of reasoning for segregation can just as well be used as a rationale for metastability of unsegregated, mixed layer structures.

Even though **S3** is more stable (by a little) than the other structures we found, we go on with examining the electronic properties of those structures—synthesis may provide those structures (or an amorphous material, see below), and the barrier to their conversion to **S3**, or complete segregation, will be large.

Amorphous and Liquid Li_4N. Intrigued by the fact that Li_4N has a rather flat energy landscape, we have constructed

DOI: 10.1021/jacs.6b09067
J. Am. Chem. Soc. 2016, 138, 14108−14120

plausible amorphous models for Li_4N using configurational bias Monte Carlo methods[96] and finite temperature molecular dynamics (MD) simulations (see Computational Methods section for details). The amorphous models built in this fashion were in turn optimized at $T \rightarrow 0$ K and $P = 1$ atm for a one-to-one comparison with Li_4N crystals. The largest model built had $Z = 48$ (am-$Li_{192}N_{48}$). Its detailed structure is shown in the SI; the model contains 5-,[97] 6-, 7-, and 8-coordinated NLi_n polyhedral units. Quite disordered, this model is only 42 meV/atom higher in energy compared to structure **1**. Other amorphous models that are energetically competent are given in the SI.

Given the melting points of Li (454 K) and Li_3N (1086 K), one would expect that of Li_4N to be intermediate between the two. We have also simulated a liquid state of Li_4N with $Z = 16$ (denoted as lq-$Li_{64}N_{16}$) by MD at 1000 K (see Computational Methods section for details), a temperature at which we think Li_4N might be liquid.

Figure 6 shows the calculated total radial distribution function (RDF) for lq-$Li_{64}N_{16}$. Those for am-$Li_{192}N_{48}$ and

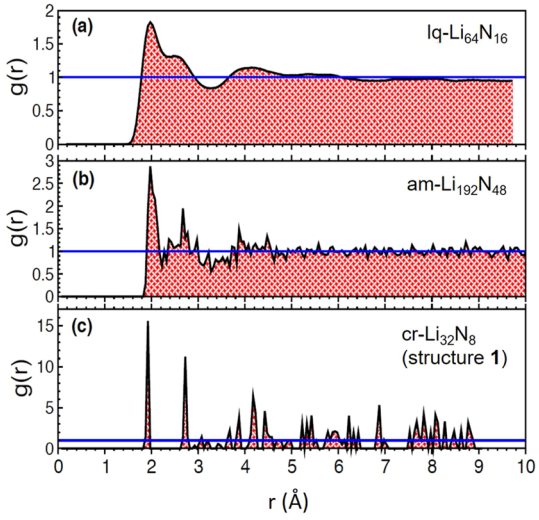

Figure 6. Total radial distribution function (RDF), $g(r)$, for (a) a liquid state of Li_4N at 1000 K (lq-$Li_{64}N_{16}$), (b) an amorphous Li_4N solid model (am-$Li_{192}N_{48}$), and (c) crystal structure **1** (cr-$Li_{32}N_8$). RDFs for am-$Li_{192}N_{48}$ and cr-$Li_{32}N_8$ are calculated for a single optimized structure, while that for lq-$Li_{64}N_{16}$ is calculated from a MD trajectory. The bin size is set to 0.05 Å.

the most stable Li_4N crystal (cr) structure **1** ($Z = 8$, *Pmma*), here called cr-$Li_{32}N_8$, are also shown. The atom-specific N−Li and Li−Li RDFs are shown in the SI. It is evident from Figure 6b that the amorphous solid model lacks long-range order, and of course, the liquid also quickly loses order as one moves to longer distances (see Figure 6a,b). On the other hand, the long-range order naturally persists in structure **1**, cr-$Li_{32}N_8$ (see Figure 6c).

Comparing RDFs with the histograms of the atom-to-atom distances in Figure 3, we see a clear agreement in the well-developed first coordination sphere, much as expected, even in the liquid state. The peak at ~2.0 Å is sharp; it corresponds to the N−Li first coordination sphere. The peak at 2.5 Å comes from the Li−Li nearest neighbors; it is rather broad, which indicates that the Li sub-lattice is more diffusive. This is consistent with ionic conductivity of Li_3N, a subject we will explore in detail elsewhere. Further analysis of atom-specific RDFs is given in the SI.

Evidence for the Electride Nature of Li_4N. *ELF First.* Determining whether a material is an electride or not is not simple. One needs to look for both valence electron density off the nuclei, and for high values of the electron localization function (ELF).[98−100] These criteria have also been suggested by Martinez-Canales et al.[31] Let us look for both in the Li_4N structures we have found.

The ELF plots for structure **1** are illustrated in Figure 7. The degree of electron localization is well gauged by ELF. The value

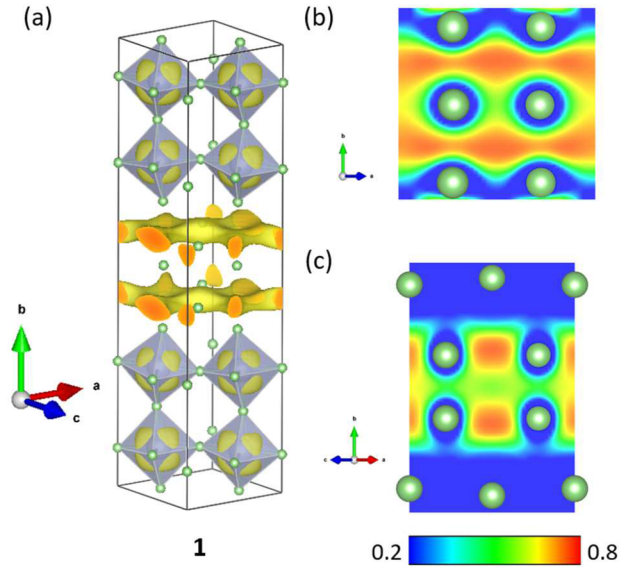

Figure 7. (a) Isosurface of ELF with the value of 0.7 for structure **1**. ELF contours of the elemental Li layer of structure **1** illustrated in the $(\bar{1}01)$ and (101) planes are shown in (b) and (c), respectively. Atoms which are not in the plane are not shown.

of ELF (usually denoted by η) is normalized in the range from 0 to 1. $\eta = 0.5$ corresponds to the homogeneous electron gas, while regions where η is close to 1 correspond to well-localized electrons, such as cores, bonds, and lone pairs.[101] Figure 7a shows the isosurface of ELF with $\eta = 0.7$. There are two different regions where electrons are localized. One is the region around the nitride ions, namely the center of NLi_6 octahedra—these are the nitride core regions. High ELF values are also found in the interstitial region, in the elemental bcc Li layer.

We scrutinize the ELF contours in the elemental Li layer in Figure 7b,c, showing two different plane cuts through the layers. In both contours we can see distinct ELF attractors (non-nuclear maxima of the electron density) located in the interstitial regions. They certainly look like a signature of an electride.

Some of ELF plots for the other structures we found are shown later, but others are shown in the SI. Briefly, we found that by the ELF criterion there is localization of electrons off the atoms in *all* the predicted Li_4N structures, including the segregated Li_4N and amorphous Li_4N structures. In the SI we discuss the ELF plots for **S3**, the most stable Li_4N structure found in this study. It shows features similar to those exhibited in Figure 7—at the boundary between the Li layer and c-Li_3N layer, there are signs of localization in the form of ELF attractors.

DOI: 10.1021/jacs.6b09067
J. Am. Chem. Soc. 2016, 138, 14108−14120

Is electride formation a general feature of metal−insulator interfaces? We intend to pursue this problem further.

Electron Densities. Let us move on to scrutiny of the electronic structure and valence electron density, to see if it contains any signs of electride formation. Figure 8a shows the

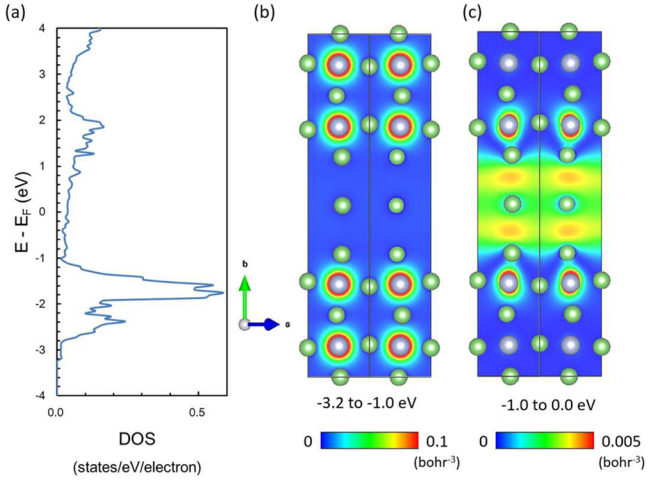

Figure 8. (a) Density of states of structure **1**. The partial charge density maps for the $(\bar{1}01)$ plane calculated using the energy ranges of -3.2 eV $\leq E \leq -1.0$ eV (b) and -1.0 eV $\leq E \leq 0.0$ eV (c). The Fermi level is located at $E = 0.0$ eV. Atoms which are not in the plane are not shown.

density of states (DOS) of structure **1**. The Fermi level is located at $E = 0$ eV. Structure **1** should be metallic; however, the DOS at the Fermi level is low. The full band structure is shown later, as are the DOS profiles of the other structures. All the calculated band structures of metastable Li_4N structural alternatives are metallic; these conclusions have been checked with "better functionals" in the SI.

We can visualize the electron density in a given energy region. So Figure 8b shows a contour map of the electron density integrated in the energy region from -3.2 to -1.0 eV. These are clearly nitride levels. More interesting is a contour map of the *partial* electron density just below the Fermi level; and integrated over the energy region from -1.0 to 0.0 eV (see Figure 8c). In this energy range, there is substantial electron density on the nitride ions in the c-Li_3N layer, but little in the other layers. We can also see very clearly four non-atom-centered electron density maxima in the elemental Li layer. These regions of off-atom density are a hallmark of electrides. One does need to examine carefully whether there may be overlap between such regions.[102] The regions where non-nuclear electron density maxima exist in this structure coincide with the regions where the ELF is high, although the maxima of ELF are not separated if we draw the isosurface of ELF with η of 0.7 or less, but diffused over the whole interlayer region (see Figure 7b). We identify the electrons in these regions as the anionic components of an electride.

In the SI we show a similar analysis for the more segregated Li_4N structure, **S3**, as well as amorphous am-$Li_{192}N_{48}$.

Classification of the Electrides Found. Figure 9 shows the DOSs of structures **2**, **3**, and **4**, chosen as representative structures of types **a**, **b**, and **c**. Structures classified as **a** and **b**, being structurally layered, are potential candidates for 2-D electrides. Those of type **c** have to be looked at one by one, for the dimensionality of the type-**c** electrides is sensitive to the

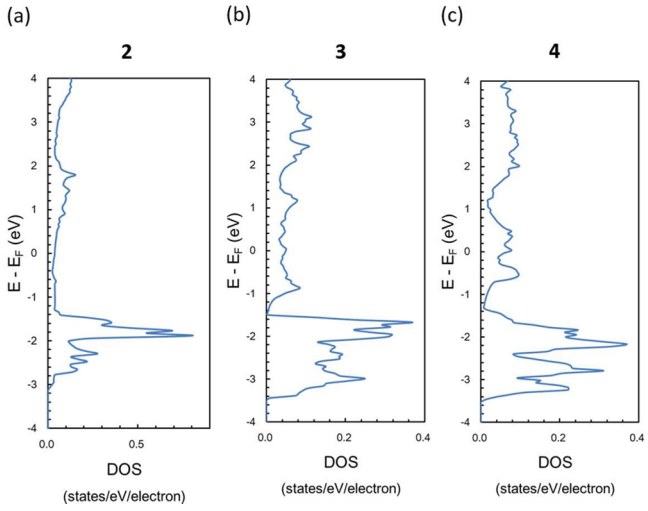

Figure 9. DOSs (per electron) of structures (a) **2**, (b) **3**, and (c) **4**.

interconnectivity of the voids in the NLi_n polyhedral network. As will be shown below, we have not found any strictly 1-D systems, but we do identify 0-D, 2-D, and 3-D electrides.

Generally the energy dependence of the DOS profile depends on the dimensionality of the system.[103] 0-D confined electrons should lead to a relatively sharp and narrow DOS peak, whereas the 2-D systems should have a typical delocalized, metallic DOS. A dependence of the DOS on $E^{-1/2}$ and $E^{1/2}$ is characteristic of 1-D and 3-D systems, respectively. We attempted to classify the Li_4N structures found on the basis of the shape of its DOS. But it turns out that things are not so simple; the nitrides also have some contribution into the region around the Fermi level, making the DOS profiles not as clear as expected.

Could the band structures be of help here? Figure 10 shows the electronic band structures for **1**, **2**, **3**, and **4**. The k-point paths were determined from the crystal symmetry by using Materials Studio;[104] the standard path for each lattice type is taken from the literature.[105]

Let us look closely at the bands in the energy range where we imagine the anionic electrons reside, namely around -1.0 to 0.0 eV. For structure **1**, around $E = -0.5$ eV, there is flat band development along Y−S; this is a path along the reciprocal space direction related to the unit cell vector perpendicular to the elemental Li layer. Significant dispersions can be seen along the other paths. This means that the anionic electrons are localized in the direction perpendicular to the Li layer, but delocalized in the Li layer. So we can designate **1** as a 2-D electride. The same is true for **2** and **3**. We observe the flat development of bands around $E = -0.4$ eV along R−X for **2** and along Y−A for **3**; the Brillouin zone (BZ) labels are different (they belong to different space-groups), but these paths are related to the direction perpendicular to the elemental Li layer in **2** and the void slab in **3**. So they are also 2-D electrides.

In structure **4** we saw voids surrounded by the NLi_8 polyhedra, so one might anticipate that this could be a 0-D electride. But it is not so in this particular case. We reproduce this large unit cell ($Z = 8$) structure below, in Figure 11a. Though the cell is large, the BZ for this space group is not so complicated (see Figure 11b). In the band structure of **4**, we do not see any significant dispersion of bands along Z−T (around $E = -0.6$ eV), S−X (around $E = -0.2$ eV), and U−R (around E

DOI: 10.1021/jacs.6b09067
J. Am. Chem. Soc. 2016, 138, 14108−14120

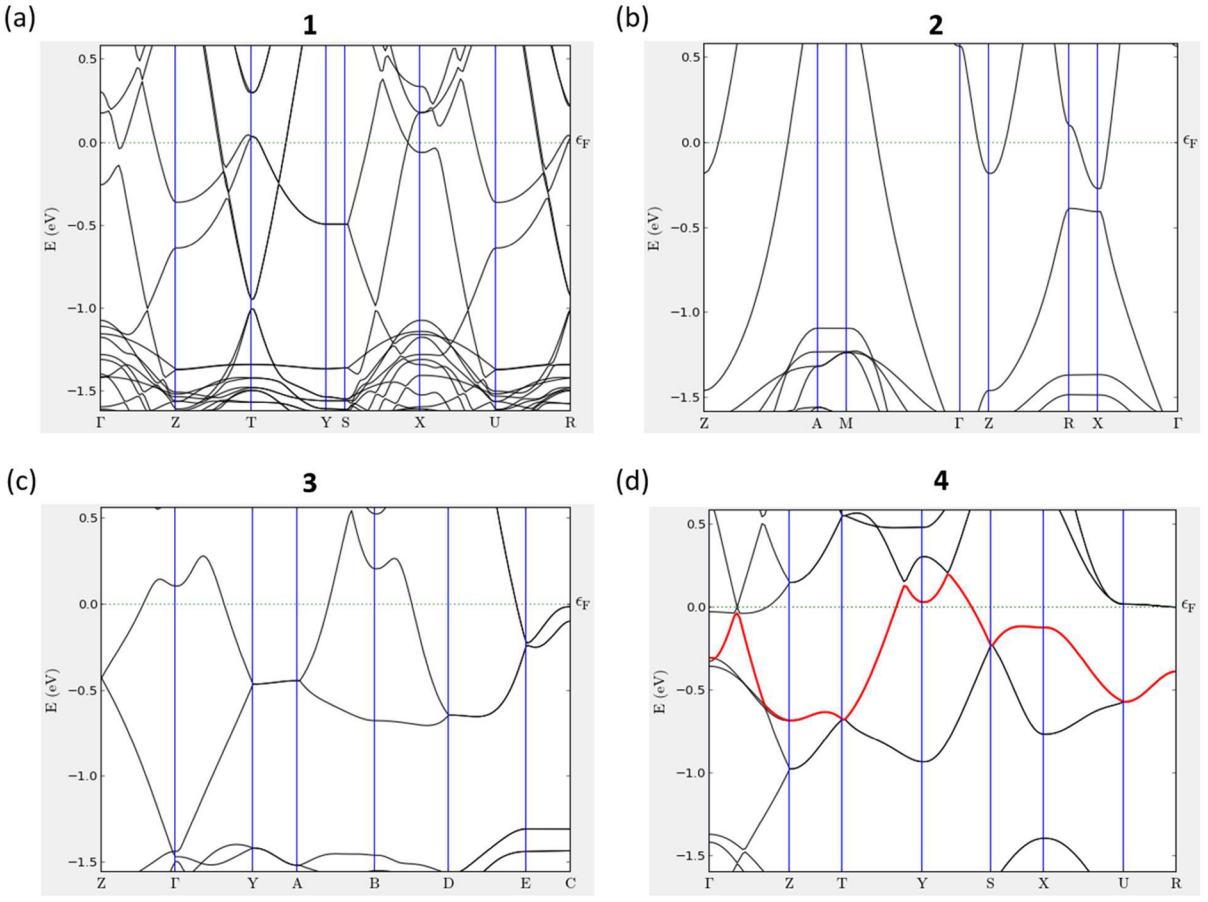

Figure 10. Electronic band structures for (a) **1**, (b) **2**, (c) **3**, and (d) **4**. The Fermi level is indicated by the green dotted line. In the band structure for **4**, the 68th band is highlighted in red (see the text for details).

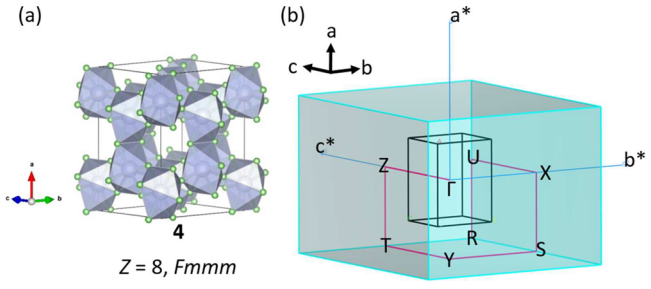

Figure 11. (a) Crystal structure of **4** reproduced and (b) lattice vectors in the orthorhombic lattice (i.e., **a**, **b**, and, **c**) and the reciprocal vectors (i.e., **a***, **b***, and, **c***) together with the high symmetry points used for the band structure calculation. The pink lines are the high symmetry lines of the first Brillouin zone. The cuboid defined by the black lines represents the real space lattice, while that defined by the light blue lines represents the reciprocal lattice.

= −0.5 eV), all of which correspond to the direction parallel to the unit cell vector **a**. On the other hand, there are significant dispersions of bands along BZ directions corresponding to the *b*- and *c*-axes, which indicates that the anionic electrons are delocalized into two directions, i.e., **b** and **c**, but confined along one direction, i.e., **a**. This leads to a conclusion that structure **4** should also be seen as a 2-D electride.

To get further insight into the electron density of **4**, we inspect the partial charge density. Since there are 136 electrons (Li: $1s^2$, $2s^1$ and N: $2s^2$, $2p^3$) in the unit cell, the 68th band (counted from the bottom) should be the highest occupied band. The 68th band is highlighted in red in Figure 10d. The band structure shows that the 68th band can be the second highest occupied band or, crossing the Fermi level, the lowest unoccupied band at some k-points. But on average it should be the highest occupied band. Figure 12 shows the contour maps

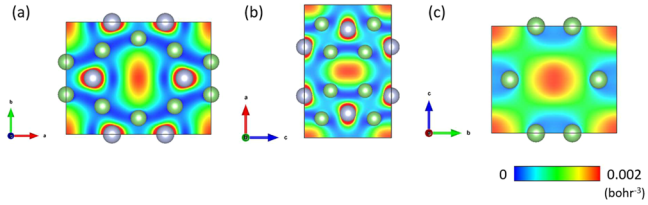

Figure 12. Contour maps of the partial charge density associated with the highest occupied band of structure **4**, which is highlighted in red in Figure 10d, in the (a) *ab*, (b) *ac*, and (c) *bc* planes. Atoms which are not in the plane are not shown.

of the partial charge density obtained by integrating the square of the absolute value of the wave function with band index 68 over all k-points. In the contour maps in the *ab* and *ac* planes (see Figure 12a and b), the non-nuclear maxima of charge density are well separated. On the other hand, the charge density between the adjacent charge density maxima in the *bc* plane (see Figure 12c) shows connecting regions of moderate density. These connecting "necks" of electron density lead to the electronic two-dimensionality of the phase, as judged by the ELF and electron density criteria.

DOI: 10.1021/jacs.6b09067
J. Am. Chem. Soc. 2016, 138, 14108−14120

In search of a 0-D electride, we investigated other type-**c** structures. Similar to structure **4**, structures **9** and **17** were also found to be electronically 2-D, and structures **8** and **23** 3-D. The details are shown in the SI.

Structure **18** finally provides the sought-for correspondence between structural and electronic dimensionality. For this phase, we can see in Figure 13b almost flat band development

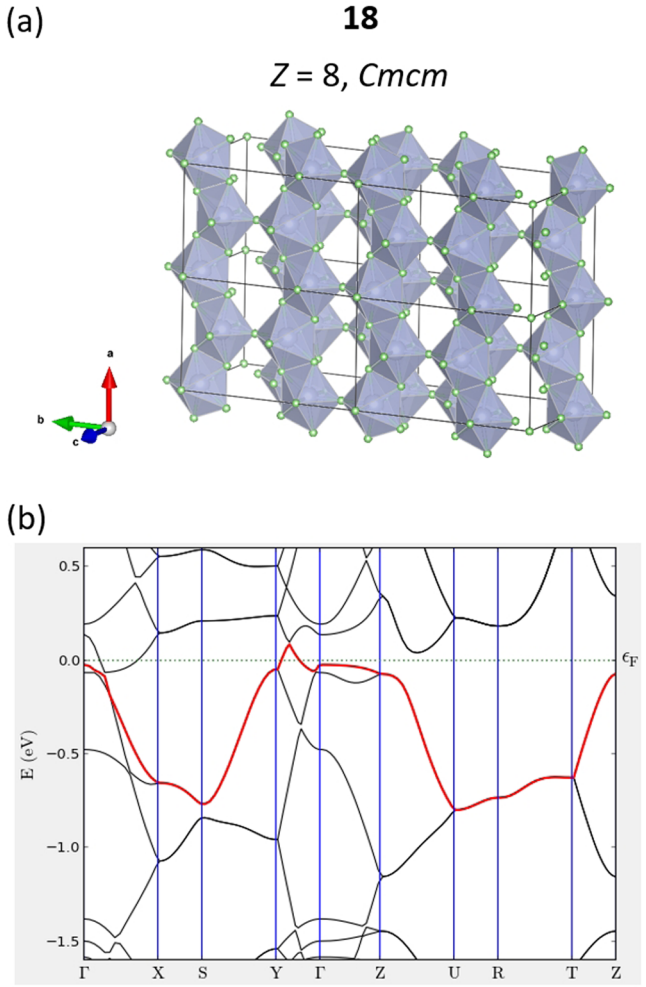

Figure 13. (a) Crystal structure of **18** shown in a 2×2×1 supercell and (b) band structure of **18**. The 68th band is highlighted in red.

at around $E = -0.7$ eV along U−R and R−T as well as just below the Fermi level along Γ−Z. The k-point paths along R−T, U−R, and Γ−Z are parallel to the unit cell vectors **a**, **b**, and **c**, respectively. This indicates that the anionic electrons in the 0-D voids are confined in all three dimensions. Such confinement is clearly shown in the partial electron density maps of **18** (see Figure 14). The regions surrounding the non-nuclear electron density maxima have low electron density, leading to well separated anionic electrons. Structure **19** (analyzed in the SI) also presents a similar picture.

SUMMARY AND CONCLUSIONS

From crystal-structure explorations of Li_4N at $P = 1$ atm, using particle swarm optimization and evolutionary algorithms, combined with DFT, there emerged 22 energetically similar but geometrically distinct and dynamically stable ground-state structures at 1 atm. We added one more structure to the list by

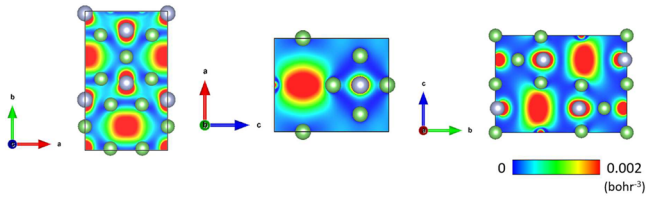

Figure 14. Contour maps of the partial charge density associated with the highest occupied band of **18**, which is highlighted in red in Figure 13b, in the *ab* (left), *ac* (center), and *bc* (right) planes. Atoms which are not in the plane are not shown.

following the imaginary phonon modes in a low-energy structure. There is much structural diversity among the structures as found. NLi_n polyhedral units, with $n = 6-9$, are common to all structures found. On the basis of the connectivity of NLi_n polyhedra, we classified the structures into three types, **a**, **b**, and **c**. Type **a** has a layered structure with alternating NLi_n polyhedral layers, as well as an elemental lithium layer. Type **b** has also a layered structure but consists only of NLi_n polyhedral layers. Type **c** has three-dimensionally interconnected NLi_n polyhedra forming more or less isolated voids.

The NLi_6 and NLi_8 polyhedra found in some of the type-**a** structures are very much akin to those in $\alpha(\alpha')$-Li_3N or c-Li_3N, which is the dominant phase in the Li−N phase diagram. This hints at a segregation of Li_4N into Li + Li_3N. In building up more segregated layers, we found an indication that segregation is energetically favorable, but not necessarily decomposition—we have checked the thermodynamic stability of Li_4N by drawing the Li-rich side of the Li−N convex-hull diagram. Li_4N structures were found to be located just on or slightly above the tie-line between Li and Li_3N. So Li_4N, stable or metastable, may exist in any of the structures we found.

Because so many structures, quite different from each other, are close (in calculations) in energy to each other, it may well be that Li_4N, when it is made, will be amorphous. Our calculation for an amorphous model also supports this conclusion. The material is also likely to be a good ionic conductor because of a very broad peak observed in the RDF for the Li−Li distances in our amorphous model.

We have investigated the electronic properties of all Li_4N structures found by plotting the band and DOS profiles. We have also scrutinized the electron localization function and partial charge density just below the Fermi level. We found that all Li_4N structures are weakly metallic. More interestingly, they show signs of being $P = 1$ atm electrides, where anionic electrons reside in the interstitial spaces, not associated with ionic cores. All type-**a** and type-**b** structures were identified as 2D electrides, as were, surprisingly given the existence of voids more or less isolated in them, some type-**c** structures. We did find two 0-D electrides, these in type-**c** structures.

COMPUTATIONAL METHODS

Li_4N structures at $P = 1$ atm were explored using both the evolutionary structure search algorithm as implemented in the XtalOpt program[88] and Crystal structure AnaLYsis by Particle Swarm Optimization methodology as implemented in the CALYPSO program.[19] All the structures obtained from these programs were optimized using DFT, as implemented in the Vienna ab initio Simulation Package (VASP).[106] The generalized gradient approximation of Perdew−Burke−Ernzerhof (PBE)[107] as the energy functional and the Projector Augmented Wave (PAW) method for the electron−ion interaction were used.[108,109] The PAW potentials represent the valence electrons of Li as $1s^2$, $2s^1$ and

DOI: 10.1021/jacs.6b09067
J. Am. Chem. Soc. 2016, 138, 14108−14120

those of N as $2s^2$, $2p^3$. A plane-wave basis set cutoff of 650 eV, self-consistent field (SCF) tolerance of 10^{-7} eV, Brillouin zone sampling on a grid of spacing $2\pi \times 0.01$ Å^{-1}, and 10^{-3} eV/Å threshold of forces on atoms guaranteed good convergence. Single-point energy calculations using a hybrid functional of HSE06[110,111] were also carried out. Since the hybrid functional calculation is very time-consuming, the k-point spacing and the SCF tolerance were increased to $2\pi \times 0.03$ Å^{-1} and 10^{-6} eV, respectively. To check the effect of dispersion interactions, calculations using Grimme's D3 dispersion correction[112] with the Becke and Johnson damping function[113] were also carried out. The phonon calculations were performed by using a supercell approach[114] with the finite displacement method as implemented in the PHONOPY code.[115] The histograms of atom-to-atom distances were generated by Distance Explorer implemented in CrystalMaker.[116] The crystal structure graphics and isosurfaces were produced using VESTA.[117] The band structure was visualized by the VNL software.[118]

The XtalOpt structure searches were carried out with system sizes containing 1, 2, and 4 formula units per simulation cell. We have followed a structure search approach similar to the one we used in our $LiNH_2$[119] and LiN_3[6a] studies. The CALYPSO structure searches were performed with system sizes containing up to four formula units per simulation cell. Each generation contains 40 structures, 60% of which are generated by particle swarm optimization and the others by random choice.

Li_4N amorphous models were constructed using configurational bias Monte Carlo methods implemented in Amorphous Cell.[96,120] The models were built upon structures **1**, **1′**, and **2** but for various Z values (number of formula units per unit cell). The shape of the unit cell considered is tetragonal, as this is the most stable lattice that we found for Li_4N crystal and the cells were loaded to a density approximately equal to the structure **1** (0.88 g/cm^3). Several approximate amorphous constructions were prepared and these were initially optimized by minimizing the close contacts between the neighboring atoms using the Universal Force Field.[121] Based on relative energies (under the force field) of the amorphous structures, lower-energy amorphous solids were screened and these again optimized with VASP using the same settings as above for Li_4N crystals.

We have carried out first-principles MD simulations for a liquid state of Li_4N. The structure was heated until it starts to melt at a pressure of ∼0 GPa and at a temperature of 1000 K. To ensure that the liquid state is obtained at that pressure, mean square displacements were calculated for the MD trajectories (see the SI). We used finite-temperature DFT with the GGA-PBE functional, as implemented in VASP. The simulations were carried out in the canonical ensemble (NVT) using Born−Oppenheimer dynamics with the Nosé−Hoover thermostat. These simulations were performed for a $2 \times 1 \times 1$ supercell of $Z = 8$, *Pmma* structure, i.e., structure **1**. Thus, the simulation cell includes totally 80 atoms. The same PAW potentials with the same plane-wave cutoff energy as mentioned above were used. The system was initially equilibrated for 1−2 ps, and subsequently simulated for 6 ps, with a time step of 0.75 fs.

■ ASSOCIATED CONTENT

Supporting Information

The Supporting Information is available free of charge on the ACS Publications website at DOI: 10.1021/jacs.6b09067.

Phonon spectra for Li_3N and Li_4N structures. Other predicted Li_4N structures with their histograms of atom-to-atom distances. The enthalpies of formation for Li_4N structures calculated with a ZPE correction, a dispersion correction, and a hybrid functional. The Li-rich side of the convex-hull diagram for the Li−N system calculated with the PBE functional, a dispersion correction, and a hybrid functional. Isosurfaces of ELF and the partial charge density associated with the highest occupied band for Li_4N structures found. Band structures and DOSs for Li_4N structures found. The DOSs of Li_4N structures calculated with hybrid functional, GW, and DFT+U methods. Analysis of the ELF and partial charge density of the more segregated Li_4N, model **S3**. Mean square displacements for the MD trajectories. Amorphous Li_4N structures obtained, and their energetics and ELF. Atom-specific N−Li and Li−Li RDFs for the liquid and amorphous models. Crystal coordinates. (PDF)

■ AUTHOR INFORMATION

Corresponding Authors

*dprasad@iitk.ac.in

*rh34@cornell.edu

Notes

The authors declare no competing financial interest.

■ ACKNOWLEDGMENTS

We gratefully acknowledge the support from the National Science Foundation through Grant CHE130587. Computational facilities from the XSEDE network (provided by the National Center for Supercomputer Applications through Grant TG-DMR060055N), KAUST (King Abdullah University of Science and Technology) Supercomputing Laboratory, EFree (an Energy Frontier Research Center funded by the Department of Energy, award no. DEC0001057 at Cornell), the IIT Kanpur Computer Centre High Performance Computing facility, IITK-HPC/RNJJ through an Initiation Grant, and Cornell's NanoScale Facility (supported by the National Science Foundation through Grant ECS-0335765) are gratefully acknowledged. Y.T. thanks the Japan Society for the Promotion of Science for a JSPS Postdoctoral Fellowship for Research Abroad.

■ REFERENCES

(1) Zintl, E.; Brauer, G. *Z. Elektrochem.* **1935**, *41*, 102−107.

(2) Pringle, G. E.; Noakes, D. E. *Acta Crystallogr., Sect. B: Struct. Crystallogr. Cryst. Chem.* **1968**, *24*, 262−269.

(3) Rabenau, A. *Solid State Ionics* **1982**, *6*, 277−293.

(4) Schulz, H.; Schwarz, K.-H. *Acta Crystallogr., Sect. A: Cryst. Phys., Diffr., Theor. Gen. Crystallogr.* **1978**, *34*, 999−1005.

(5) Fair, H. D.; Walker, R. F. *Energetic Materials, Physics and Chemistry of the Inorganic Azides*; Plenum Press: New York, 1977; Vol. *1*.

(6) For studies of lithium azide under pressure, see: (a) Prasad, D. L. V. K.; Ashcroft, N. W.; Hoffmann, R. *J. Phys. Chem. C* **2013**, *117*, 20838−20846. (b) Wang, X.; Li, J.; Botana, J.; Zhang, M.; Zhu, H.; Chen, L.; Liu, H.; Cui, T.; Miao, M. *J. Chem. Phys.* **2013**, *139*, 164710.

(7) Schneider, S. B.; Frankovsky, R.; Schnick, W. *Angew. Chem., Int. Ed.* **2012**, *51*, 1873−1875.

(8) (a) See references in ref 7. The early papers here are the following:. (b) Auffermann, G.; Prots, Y.; Kniep, R. *Angew. Chem.* **2001**, *113*, 565−567; *Angew. Chem., Int. Ed.* **2001**, *40*, 547−549. (c) Vajenine, G. V.; Auffermann, G.; Prots, Y.; Schnelle, W.; Kremer, R. K.; Simon, A.; Kniep, R. *Inorg. Chem.* **2001**, *40*, 4866−4870. (d) Auffermann, G.; Kniep, R.; Bronger, W. *Z. Anorg. Allg. Chem.* **2006**, *632*, 565−571. (e) Prots, Y.; Auffermann, G.; Tovar, M.; Kniep, R. *Angew. Chem.* **2002**, *114*, 2392−2394; *Angew. Chem., Int. Ed.* **2002**, *41*, 2288−2290.

(9) Alpen, U. v. *J. Solid State Chem.* **1979**, *29*, 379−392.

(10) Schulz, H.; Thiemann, K. H. *Acta Crystallogr., Sect. A: Cryst. Phys., Diffr., Theor. Gen. Crystallogr.* **1979**, *35*, 309−314.

(11) Schneider, S. B.; Mangstl, M.; Friederichs, G. M.; Frankovsky, R.; Schmedt auf der Gunne, J.; Schnick, W. *Chem. Mater.* **2013**, *25*, 4149−4155.

(12) Yonco, R. M.; Veleckis, E.; Maroni, V. A. *J. Nucl. Mater.* **1975**, *57*, 317−324.

(13) Adams, P. F.; Hubberstey, P.; Pulham, R. J. *J. Less-Common Met.* **1975**, *42*, 1−11.
(14) Sangster, J.; Pelton, A. D. *J. Phase Equilib.* **1992**, *13*, 291−296.
(15) Wang, W. J.; Yuan, W. X.; Song, Y. T.; Chen, X. L. *J. Alloys Compd.* **2003**, *352*, 103−105.
(16) (a) Oganov, A. R., Ed. *Modern Methods of Crystal Structure Prediction*; Wiley-VCH: Weinheim, 2011. (b) Atahan-Evrenk, S.; Aspuru-Guzik, A. *Prediction and Calculation of Crystal Structures*; Springer: New York, 2014.
(17) Peng, F.; Yao, Y.; Liu, H.; Ma, Y. *J. Phys. Chem. Lett.* **2015**, *6*, 2363−2366.
(18) Shen, Y.; Oganov, A. R.; Qian, G.; Zhang, J.; Dong, H.; Zhu, Q.; Zhou, Z. *Sci. Rep.* **2015**, *5*, 14204.
(19) Wang, Y.; Lv, J.; Zhu, L.; Ma, Y. *Phys. Rev. B: Condens. Matter Mater. Phys.* **2010**, *82*, 094116.
(20) Glass, C. W.; Oganov, A. R.; Hansen, N. *Comput. Phys. Commun.* **2006**, *175*, 713−720.
(21) Zhang, X.; Zunger, A.; Trimarchi, G. *J. Chem. Phys.* **2010**, *133*, 194504.
(22) Hosono, H.; Mishima, Y.; Takezoe, H.; MacKenzie, K. J. D. *Nanomaterials: Research Towards Applications*; Elsevier Science: Amsterdam, 2006.
(23) Wagner, M. J.; Huang, R. H.; Eglin, J. L.; Dye, J. L. *Nature* **1994**, *368*, 726−729.
(24) Dye, J. L. *Acc. Chem. Res.* **2009**, *42*, 1564−1572 and references therein.
(25) Simon, A. *Coord. Chem. Rev.* **1997**, *163*, 253−270.
(26) Kim, S. W.; Shimoyama, T.; Hosono, H. *Science* **2011**, *333*, 71−74.
(27) Lee, K.; Kim, S. W.; Toda, Y.; Matsuishi, S.; Hosono, H. *Nature* **2013**, *494*, 336−340.
(28) Karpov, A.; Wedig, U.; Dinnebier, R. E.; Jansen, M. *Angew. Chem., Int. Ed.* **2005**, *44*, 770−773.
(29) Zurek, E.; Edwards, P. P.; Hoffmann, R. *Angew. Chem., Int. Ed.* **2009**, *48*, 8198−8232 and references therein.
(30) Pickard, C. J.; Needs, R. J. *Phys. Rev. Lett.* **2009**, *102*, 146401.
(31) Martinez-Canales, M.; Pickard, C. J.; Needs, R. J. *Phys. Rev. Lett.* **2012**, *108*, 045704.
(32) Ma, Y.; Eremets, M.; Oganov, A. R.; Xie, Y.; Trojan, I.; Medvedev, S.; Lyakhov, A. O.; Valle, M.; Prakapenka, V. *Nature* **2009**, *458*, 182−185.
(33) Von Schnering, H. G.; Nesper, R. *Angew. Chem., Int. Ed. Engl.* **1987**, *26*, 1059−1200.
(34) Li, P.; Gao, G.; Wang, Y.; Ma, Y. *J. Phys. Chem. C* **2010**, *114*, 21745−21749.
(35) Hayes, W.; Stoneham, A. M. *Defects and Defect Processes in Nonmetallic Solids*; Wiley: New York, 1985.
(36) Miao, M. S.; Hoffmann, R. *Acc. Chem. Res.* **2014**, *47*, 1311−1317 and references therein.
(37) Miao, M.-S.; Hoffmann, R. *J. Am. Chem. Soc.* **2015**, *137*, 3631−3637.
(38) Torrisi, A. *Opticon1826* **2011**, *11*, 1−5.
(39) Dye, J. L. *Philos. Trans. R. Soc., A* **2015**, *373*, 20140174.
(40) Kraus, C. *J. Am. Chem. Soc.* **1908**, *30*, 1323−1344.
(41) Ellaboudy, A.; Dye, J. L.; Smith, P. B. *J. Am. Chem. Soc.* **1983**, *105*, 6490−6491.
(42) Wagner, M. J.; Dye, J. L. *Annu. Rev. Mater. Sci.* **1993**, *23*, 223−253.
(43) Redko, M. Y.; Jackson, J. E.; Huang, R. H.; Dye, J. L. *J. Am. Chem. Soc.* **2005**, *127*, 12416−12422.
(44) Ichimura, A. S.; Dye, J. L.; Camblor, M. A.; Villaescusa, L. A. *J. Am. Chem. Soc.* **2002**, *124*, 1170−1171.
(45) Li, Z.; Yang, J.; Hou, J. G.; Zhu, Q. *J. Am. Chem. Soc.* **2003**, *125*, 6050−6051.
(46) Matsuishi, S.; Toda, Y.; Miyakawa, M.; Hayashi, K.; Kamiya, T.; Hirano, M.; Tanaka, I.; Hosono, H. *Science* **2003**, *301*, 626−629.
(47) Sushko, P. V.; Shluger, A. L.; Hirano, M.; Hosono, H. *J. Am. Chem. Soc.* **2007**, *129*, 942−951.
(48) Gregory, D. H.; Bowman, A.; Baker, C. F.; Weston, D. P. *J. Mater. Chem.* **2000**, *10*, 1635−1641 and references therein.
(49) Walsh, A.; Scanlon, D. O. *J. Mater. Chem. C* **2013**, *1*, 3525−3528.
(50) Schleyer, P. v. R. In *New Horizons of Quantum Chemistry*; Lowdin, P.-O., Pullman, B., Eds.; Proceedings of the Fourth International Congress of Quantum Chemistry, Uppsala, Sweden, 1982; D. Reidel Publishing Co.: Dordrecht, The Netherlands, 1983; pp 95−109.
(51) Sushko, P. V.; Shluger, A. L.; Hayashi, K.; Hirano, M.; Hosono, H. *Mater. Sci. Eng., C* **2005**, *25*, 722−726.
(52) Zhang, X.; Xiao, Z.; Lei, H.; Toda, Y.; Matsuishi, S.; Kamiya, T.; Ueda, S.; Hosono, H. *Chem. Mater.* **2014**, *26*, 6638−6643.
(53) Zhang, Y. Q.; Xiao, Z. W.; Kamiya, T.; Hosono, H. *J. Phys. Chem. Lett.* **2015**, *6*, 4966−4971.
(54) Lu, Y.; Li, J.; Tada, T.; Toda, Y.; Ueda, S.; Yokoyama, T.; Kitano, M.; Hosono, H. *J. Am. Chem. Soc.* **2016**, *138*, 3970−3973.
(55) Toda, Y.; Yanagi, H.; Ikenaga, E.; Kim, J. J.; Kobata, M.; Ueda, S.; Kamiya, T.; Hirano, M.; Kobayashi, K.; Hosono, H. *Adv. Mater.* **2007**, *19*, 3564−3569.
(56) Michaelson, H. B. *J. Appl. Phys.* **1977**, *48*, 4729−4733.
(57) Kitano, M.; Inoue, Y.; Yamazaki, Y.; Hayashi, F.; Kanbara, S.; Matsuishi, S.; Yokoyama, T.; Kim, S.-W.; Hara, M.; Hosono, H. *Nat. Chem.* **2012**, *4*, 934−940.
(58) Toda, Y.; Hirayama, H.; Kuganathan, N.; Torrisi, A.; Sushko, P. V.; Hosono, H. *Nat. Commun.* **2013**, *4*, 2378.
(59) Hayashi, F.; Kitano, M.; Yokoyama, T.; Hara, M.; Hosono, H. *ChemCatChem* **2014**, *6*, 1317−1323.
(60) Kim, Y. J.; Kim, S. M.; Hosono, H.; Yang, J. W.; Kim, S. W. *Chem. Commun.* **2014**, *50*, 4791−4794.
(61) Kuganathan, N.; Hosono, H.; Shluger, A. L.; Sushko, P. V. *J. Am. Chem. Soc.* **2014**, *136*, 2216−2219.
(62) Nakamura, N.; Watanabe, T.; Kim, J.; Watanabe, S.; Matsuzaki, E.; Toda, Y.; Miyakawa, N.; Fujitsu, S.; Hosono, H. *Dig. Tech. Pap. - Soc. Inf. Disp. Int. Symp.* **2015**, *46*, 1710−1713.
(63) Xu, H. L.; Li, Z. R.; Wu, D.; Wang, B. Q.; Li, Y.; Gu, F. L.; Aoki, Y. *J. Am. Chem. Soc.* **2007**, *129*, 2967−2970.
(64) He, H.-M.; Li, Z.-R.; Li, Y.; Sun, W.-M.; Wang, J.-J.; Liu, J.-y.; Wu, D. *J. Phys. Chem. C* **2014**, *118*, 23937−23945.
(65) Hu, J.; Xu, B.; Yang, S. A.; Guan, S.; Ouyang, C.; Yao, Y. *ACS Appl. Mater. Interfaces* **2015**, *7*, 24016−24022.
(66) Hosono, H. *Phys. C* **2009**, *469*, 314−325.
(67) He, Y. *J. Alloys Compd.* **2016**, *654*, 180−184.
(68) Lu, M.; Zhang, M.; Liu, H. *Phys. Lett. A* **2015**, *379*, 2511−2514.
(69) Inoshita, T.; Jeong, S.; Hamada, N.; Hosono, H. *Phys. Rev. X* **2014**, *4*, 031023.
(70) Tada, T.; Takemoto, S.; Matsuishi, S.; Hosono, H. *Inorg. Chem.* **2014**, *53*, 10347−10358.
(71) Zhang, Y.; Wang, H.; Wang, Y.; Zhang, L.; Ma, Y. *arXiv* **2016**, *1603*, 04161.
(72) Zhu, Q.; Oganov, A. R.; Lyakhov, A. O. *Phys. Chem. Chem. Phys.* **2013**, *15*, 7696−7700.
(73) Dong, X.; Oganov, A. R.; Goncharov, A. F.; Stavrou, E.; Lobanov, S.; Saleh, G.; Qian, G. R.; Zhu, Q.; Gatti, C.; Zhou, X. F. *arXiv* **2013**, *1309*, 3827.
(74) Dong, X.; Li, Y.-L.; Oganov, A. R.; Li, K.; Zheng, H.; Mao, H.-k. *arXiv* **2016**, *1603*, 02880.
(75) Kokail, C.; Heil, C.; Boeri, L. *Phys. Rev. B: Condens. Matter Mater. Phys.* **2016**, *94*, 060502.
(76) Gao, Y.; Wu, H. Q.; Sun, S. L.; Xu, H. L.; Su, Z. M. *J. Mol. Model.* **2015**, *21*, 23.
(77) Postils, V.; Garcia-Borràs, M.; Solà, M.; Luis, J. M.; Matito, E. *Chem. Commun.* **2015**, *51*, 4865−4868.
(78) Liang, W.-M.; Zhao, Z.-X.; Wu, D.; Sun, W.-M.; Li, Y.; Li, Z.-R. *J. Mol. Model.* **2015**, *21*, 311.
(79) Simons, J.; Gutowski, M. *Chem. Rev.* **1991**, *91*, 669−677.
(80) Dale, S. G.; Otero-de-la Roza, A.; Johnson, E. R. *Phys. Chem. Chem. Phys.* **2014**, *16*, 14584−14593.

DOI: 10.1021/jacs.6b09067
J. Am. Chem. Soc. 2016, 138, 14108−14120

(81) Janesko, B. G.; Scalmani, G.; Frisch, M. J. *J. Chem. Theory Comput.* **2016**, *12*, 79−91.
(82) Simon, A. *Struct. Bonding (Berlin, Ger.)* **1979**, *36*, 81−127.
(83) Wu, G.; Wu, S.; Wu, P. *Phys. Rev. Lett.* **2011**, *107*, 118302.
(84) Schön, J. C.; Wevers, M. A. C.; Jansen, M. *J. Mater. Chem.* **2001**, *11*, 69−77.
(85) Nguyen, M. C.; Hoang, K.; Wang, C.-Z.; Ho, K.-M. *Phys. Chem. Chem. Phys.* **2016**, *18*, 4185−4190.
(86) Shannon, R. *Acta Crystallogr., Sect. A: Cryst. Phys., Diffr., Theor. Gen. Crystallogr.* **1976**, *32*, 751−767.
(87) Fischer, D.; Jansen, M. *Angew. Chem., Int. Ed.* **2002**, *41*, 1755−1756.
(88) Lonie, D.; Zurek, E. *Comput. Phys. Commun.* **2011**, *182*, 372−387.
(89) Venables, J. A.; English, C. A. *Acta Crystallogr., Sect. B: Struct. Crystallogr. Cryst. Chem.* **1974**, *30*, 929−935.
(90) Nadler, M. R.; Kempier, C. P. *Anal. Chem.* **1959**, *31*, 2109−2109.
(91) Smith, H. G. *Phys. Rev. Lett.* **1987**, *58*, 1228−1231.
(92) Overhauser, A. W. *Phys. Rev. Lett.* **1984**, *53*, 64−65.
(93) Doll, K.; Harrison, N. M.; Saunders, V. R. *J. Phys.: Condens. Matter* **1999**, *11*, 5007−5019.
(94) Kulkarni, A.; Doll, K.; Prasad, D. L. V. K.; Schön, J. C.; Jansen, M. *Phys. Rev. B: Condens. Matter Mater. Phys.* **2011**, *84*, 172101.
(95) According to eq 1, when we use bcc Li as a reference, the formation enthalpy of Li_4N can be calculated as $\Delta H_f(Li_4N) = {}^1/_5H(Li_4N) - {}^4/_5H(\text{bcc Li}) - {}^1/_5H(N)$. On the other hand, if we use 9R Li, the formation enthalpy is $\Delta H'_f(Li_4N) = {}^1/_5H(Li_4N) - {}^4/_5H(\text{9R Li}) - {}^1/_5H(N)$. The difference between these enthalpies is $\Delta H'_f(Li_4N) - \Delta H_f(Li_4N) = {}^4/_5[H(\text{bcc Li}) - H(\text{9R Li})] = {}^4/_5 \times 1.5$ meV/atom = 1.2 meV/atom.
(96) Akkermans, R. L. C.; Spenley, N. A.; Robertson, S. H. *Mol. Simul.* **2013**, *39*, 1153−1164.
(97) If we set a threshold distance of the radius of coordination sphere around the nitride ions to 2.1 Å, we observe 5-coordinated NLi_n polyhedra. However, if we increase the threshold value, we observe that more lithiums coordinate to the nitride ions. It is also true for α-Li_3N, where one can see 2-coordinated nitride ions for the threshold distance of 1.9 Å and 8-coordinated ones for 2.1 Å. So within that small range of distance, the coordination number varies.
(98) Becke, A. D.; Edgecombe, K. E. *J. Chem. Phys.* **1990**, *92*, 5397−5403.
(99) Savin, A.; Nesper, R.; Wengert, S.; Fassler, T. F. *Angew. Chem., Int. Ed. Engl.* **1997**, *36*, 1808−1832.
(100) Sattler, K. D., Ed. *Handbook of Nanophysics, Principles and Methods*; CRC Press: Boca Raton, FL, 2011.
(101) Savin, A.; Becke, A. D.; Flad, J.; Nesper, R.; Preuss, H.; von Schnering, H. G. *Angew. Chem., Int. Ed. Engl.* **1991**, *30*, 409−412.
(102) Zhao, S.; Kan, E.; Li, Z. *WIREs Comput. Mol. Sci.* **2016**, *6*, 430−440.
(103) Schubert, E. F. *Physical Foundations of Solid-State Devices*; Rensselaer Polytechnic Institute: New York, 2015.
(104) *Materials Studio*, version 8; Accelrys Inc.: San Diego, CA, 2014.
(105) Bradley, C. J.; Cracknell, A. P. *Mathematical Theory of Symmetry in Solids*; Oxford University Press: Oxford, U.K., 1972.
(106) Kresse, G.; Furthmüller, J. *Phys. Rev. B: Condens. Matter Mater. Phys.* **1996**, *54*, 11169.
(107) Perdew, J. P.; Burke, K.; Ernzerhof, M. *Phys. Rev. Lett.* **1996**, *77*, 3865−3868.
(108) Blöchl, P. E. *Phys. Rev. B: Condens. Matter Mater. Phys.* **1994**, *50*, 17953−17979.
(109) Kresse, G.; Joubert, D. *Phys. Rev. B: Condens. Matter Mater. Phys.* **1999**, *59*, 1758−1775.
(110) Heyd, J.; Scuseria, G. E.; Ernzerhof, M. *J. Chem. Phys.* **2003**, *118*, 8207−8215.
(111) Heyd, J.; Scuseria, G. E.; Ernzerhof, M. *J. Chem. Phys.* **2006**, *124*, 219906.
(112) Grimme, S.; Antony, J.; Ehrlich, S.; Krieg, H. *J. Chem. Phys.* **2010**, *132*, 154104.
(113) Johnson, E. R.; Becke, A. D. *J. Chem. Phys.* **2006**, *124*, 174104.
(114) Parlinski, K.; Li, Z. Q.; Kawazoe, Y. *Phys. Rev. Lett.* **1997**, *78*, 4063.
(115) Togo, A.; Oba, F.; Tanaka, I. *Phys. Rev. B: Condens. Matter Mater. Phys.* **2008**, *78*, 134106.
(116) *CrystalMaker Software Ltd.*, www.crystalmaker.com.
(117) Momma, K.; Izumi, F. *J. Appl. Crystallogr.* **2011**, *44*, 1272−1276.
(118) *QuantumWise*, http://quantumwise.com.
(119) Prasad, D. L. V. K.; Ashcroft, N. W.; Hoffmann, R. *J. Phys. Chem. A* **2012**, *116*, 10027−10036.
(120) Flory, P. J. *Statistical Mechanics of Chain Molecules*; Hanser Publishers: New York, 1988.
(121) Rappé, A. K.; Casewit, C. J.; Colwell, K. S.; Goddard, W. A.; Skiff, V. M. *J. Am. Chem. Soc.* **1992**, *114*, 10024−10035.

DOI: 10.1021/jacs.6b09067
J. Am. Chem. Soc. 2016, 138, 14108−14120